Eksploatacja i Niezawodnosc – Maintenance and Reliability
Volume 23 (2021), Issue 4
journal homepage: http://www.ein.org.pl
Article citation info:
Jedliński Ł. Influence of the movement of involute profile gears along the off-line of action on the gear tooth position along the line of action direction. Eksploatacja i Niezawodnosc – Maintenance and Reliability 2021; 23 (4): 736–744, http://doi.org/10.17531/ein.2021.4.16.

Influence of the movement of involute profile gears along the off-line of action on the gear tooth position along the line of action direction

Indexed by: Web of Science Group

Łukasz Jedliński[a]

[a] Lublin University of Technology, ul. Nadbystrzycka 36, 20-618 Lublin, Poland

Highlights

- Algorithm for finding the exact value of normal backlash is presented.
- Influence of gear parameters on normal backlash for gear OLOA displacement is checked.
- Dynamic simulation is performed and several aspects are analyzed.

Abstract

When gears change their distance along the off-line of action (OLOA) direction, this affects the distance between the working surfaces of the meshing teeth along the line of action (LOA). This effect is usually neglected in studies. To include this effect precise equations are derived for spur gears. The analysis is carried out for the general case of spur gears with shifted profiles frequently used in the industry. The influence of OLOA gear displacement on LOA direction is also a function of gears parameters. An analysis is conducted, and the impact of parameters such as module, pressure angle, gear ratio, and the number of teeth is determined. As an example, a simulation of a 12 DOF analytical model is presented. The movement of gears along OLOA is caused by a frictional force that can be high during tooth degradation e.g. scuffing. Results show that when the movement of gears along the OLOA direction is significant, its influence on the distance between the mating teeth should not be neglected.

Keywords

normal backlash, analytical model, OLOA movement, bearing reactions, dynamic meshing force.

This is an open access article under the CC BY license (https://creativecommons.org/licenses/by/4.0/)

1. Introduction

A general trend in simulation models for mechanisms and machines is to achieve an accurate solution in acceptable time. Gears and gear units are very often analyzed because of their importance [3, 26]. Analytical models are efficient and based on basic principles ensuring the correctness of results for a given condition [5]. Mechanisms are very often described by equations of motion that do not have an exact solution [18]. In effect, numerical methods must be employed to resolve this problem, and numerical models can be called as semi-analytical. Numerical models are very popular, the dominant numerical technique being finite element analysis (FEA) [16]. FEA models are usually very detailed and can include different types of phenomena. A disadvantage of these models is their very long computation time. To overcome this drawback, hybrid models [12] are used.

All model types are developed to minimize their disadvantages. In this study, analytical formulas are derived to describe spur gears in a more precise and detailed way that can be used in analytical, semi-analytical and hybrid models. A common practice in modeling is to orient the axes of a coordinate system according to the line of action (LOA) and off-line of action (OLOA). This simplifies calculations because then both the normal force and the friction force do not consist of two components. Also, if the center distance is changed along LOA, the same displacement is made between the surfaces of the involute profile teeth that are in mesh. As far as gear movement along OLOA is concerned, its impact on the meshing tooth surface distance is neglected in most studies [4, 6, 17, 21, 24, 27]. In this study, the relationship between the varying distance of gears along OLOA and its effect on the distance between the teeth in mesh is established. Obtained equations are precise for involute gears and no simplifications were made to derive them. To the author's best knowledge, this is a novel solution.

In some studies, the problem of varying center distance and its influence on gear parameters is investigated. A change in the distance between the mating teeth can be considered as varying backlash. In the LOA direction it is normal backlash. In study [13] a single stage spur gear is analyzed. Geometric eccentricity and its influence on backlash are considered. The change in backlash is calculated according to the formula $\Delta b = (r_{b1} + r_{b2})\mathrm{inv}(\alpha) - (r_{b1} + r_{b2})\mathrm{inv}(\alpha')$ where α is the theoretical meshing angle and the theoretical meshing angle α' is 20°. The term "meshing angle" is ambiguous. This formula is also used in [25] and the previous study is quoted as a source. In the study, bearing deformation is the reason for changing the center distance and the influence on backlash is included. Time-varying backlash is defined as $\Delta b = 2(R_1 + R_2)(\mathrm{inv}(\alpha) - \mathrm{inv}(\alpha_0))$ where Δb is the dynamic backlash, α_0 denotes the initial pressure angle for the initial center distance d_0, $\alpha = \cos^{-1}((R_1 + R_2)/d)$ is the actual pressure

E-mail addresses: Ł. Jedliński - l.jedlinski@pollub.pl

angle. According to these equations, the backlash Δb depends on two parameters: the pressure angle and the center distance. This formula is, however, incorrect. For simplicity, let us consider the movement of one gear. Along the LOA direction, changes in center distance and pressure angle are not significant but have the greatest impact on backlash. In contrast, the movement of a gear along the OLOA direction has a significant impact on center distance and pressure angle, but its impact on backlash is minimal. This stands in contradiction with the above formula, and results will differ by several orders of magnitude, according to the author's calculations. In [7] the effect of eccentricity on backlash is investigated. Time-varying backlash for a driving gear caused by eccentricity is expressed as $\Delta b = -2e_1 \cos(\theta_1 \pm \varphi_1) \tan\alpha$, where e and θ are the gear eccentricity and its initial phase, φ is the angular displacement of gear, and α is the pressure angle. This is a simplified equation. Pressure angle is maintained constant and changes in backlash do not have an exact cosine shape. According to Fig. 1 given in the reference article, the initial phase angle θ is measured from the line which connects the axes of gear rotation. Assuming that θ_1 and φ_1 are equal to 0, the displacement of gears will take place along a direction passing through the axes of rotation. Backlash will reach the maximum value, which is not the case with involute gears. Large bearing clearance and variations in backlash were reported in [14]. The relationship between center distance and backlash was established with approximation of tooth profile. The involute curve was treated as a line. A planetary gear unit used in a turbo-fan engine is studied in [22]. The model presented in the work is comprehensive and many of its parameters are made depended on time. One of them is backlash. The authors derived the formula for calculating backlash from [13], which is incorrect.

From the above paragraph, it can be concluded that information about normal backlash as a function of gear displacement is of vital importance for the model to be more accurate and comprehensive. The relationship between the movement of gears along OLOA and the distance between the mating tooth surface along LOA (changes in normal backlash) is especially important when the movement (displacement) of gears along OLOA is considerable. Suitable conditions are ensured when e.g. bearing clearance, eccentric gear movement and high friction force are considered in analysis. These three cases will be discussed for different displacement values. An analysis of a rotor-bearing-pedestal system was presented by Cao et al. [1]. With the bearing fit clearance equal to 10 μm and unbalance mass on the rotor, the axis orbit can have a diameter of about 60 μm. The problem of clearance between the rolling bearing outer ring and housing was modelled and analyzed by Chen and Qu [2], who considered a fit clearance of up to 500 μm. Radial internal clearance in the rolling bearing was set to 20 μm in [19, 20]. In a model for analyzing the vibration behavior of a rotor-bearing system, Wang and Zhu [23] set an internal clearance of the cylindrical roller bearing at 60 μm in compliance with ISO 5753-1:2009. Grade accuracy has a great impact on the runout of gears. According to the ISO 1328-2 Cylindrical gears – ISO system of accuracy [9], the runout for gears with a diameter of up to 125 mm can amount to about 200 μm for grade 12. Variations in the center distance reported in [25] amount up to 30 μm and those reported in [22] up to 120 μm. The gear friction coefficient is high when failure occurs. Insufficient lubrication or lack thereof may be its cause. This can lead to scuffing [8, 15]. During this process the friction coefficient has a high value.

For these reasons, it is important to take into account the influence of gear movement along OLOA on distance between the meshing teeth along the LOA direction (normal backlash). An accurate algorithm is derived and an analysis is carried out. In the first simulation the impact of gear parameters such as module, pressure angle, gear ratio and the number of teeth on the distance between the meshing teeth is examined. The other simulation compares results obtained with and without taking into account the movement of gears along OLOA on the dynamic meshing force and bearing force.

Nomenclature

T_m – input motor torque [Nm]

T_d – output device torque [Nm]

I_m – mass moment of inertia of the motor rotor and half of coupling [kg m^2]

I_p – mass moment of inertia of the pinion, shaft and half of coupling (pinion subassembly) [kg m^2]

I_g – mass moment of inertia of the gear, shaft and half of coupling (gear subassembly) [kg m^2]

I_d – mass moment of inertia of the device rotor and half of coupling [kg m^2]

I_{px} ($I_{px} = I_{py}$) – mass moment of inertia of the pinion, shaft and half of coupling about y_{op} axis [kg m^2]

I_{gx} ($I_{gx} = I_{gy}$) – mass moment of inertia of the gear, shaft and half of coupling about the y_{og} axis [kg m^2]

$\ddot{\varphi}$ – angular acceleration [rad/ s^2]: $\ddot{\varphi}_m$ – motor rotor, $\ddot{\varphi}_p$ – pinion, $\ddot{\varphi}_g$ – gear, $\ddot{\varphi}_d$ – device rotor

$\ddot{\theta}_{px}$ – angular acceleration of the pinion about the y_{op} axis [rad/ s^2]

$\ddot{\theta}_{gx}$ – angular acceleration of the gear about the y_{og} axis [rad/ s2]

$\ddot{\theta}_{py}$ – angular acceleration of the pinion about the x_{op} axis [rad/ s2]

$\ddot{\theta}_{py}$ – angular acceleration of the gear about the x_{og} axis [rad/s2]

$\ddot{x}_p$ – linear acceleration of the pinion on plane defined by the x_{op} axis and pinion axis of rotation [m/s^2]

$\ddot{x}_g$ – linear acceleration of the gear on plane defined by the x_{og} axis and gear axis of rotation [m/s2]

x_{py} – distance between new contact point and pinion tooth flank along LOA (x) caused by the movement of gears along OLOA (y) [m],

x_{gy} – distance between new contact point and gear tooth flank along LOA (x) caused by the movement of gears along OLOA (y) [m],

$\ddot{y}_p$ – linear acceleration of the pinion on plane defined by the y_{op} axis and pinion axis of rotation [m/s^2]

$\ddot{y}_g$ – linear acceleration of the gear on plane defined by the y_{og} axis and gear axis of rotation [m/s^2]

$M_{cm} = c_m\left(\dot{\varphi}_m - \dot{\varphi}_p\right)r_m$ – torque applied on the motor coupling from damping [Nm]

$M_{km} = k_m\left(\varphi_m - \varphi_p\right)r_m$ – torque applied on the motor coupling from stiffness [Nm]

$M_{cp} = c\left(r_{b1}\dot{\varphi}_p + \dot{x}_p - \dot{x}_{py} - r_{b2}\dot{\varphi}_g + \dot{x}_g - \dot{x}_{gy}\right)r_{b1}$ – torque applied on the pinion from damping [Nm]

$M_{kp} = k\left(r_{b1}\varphi_p + x_p - x_{py} - r_{b2}\varphi_g + x_g - x_{gy}\right)r_{b1}$ – torque applied on the pinion from stiffness [Nm]

$M_{kg} = k\left(r_{b1}\varphi_p + x_p - x_{py} - r_{b2}\varphi_g + x_g - x_{gy}\right)r_{b2}$ – torque applied on the gear from damping [Nm]

$M_{kg} = k\left(r_{b1}\varphi_p + x_p - x_{py} - r_{b2}\varphi_g + x_g - x_{gy}\right)r_{b2}$ – torque applied on the gear from stiffness [Nm]

$M_{cd} = c_d\left(\dot{\varphi}_g - \dot{\varphi}_d\right)r_d$ – torque applied on the device coupling from damping [Nm]

$M_{kd} = k_d\left(\varphi_g - \varphi_d\right)r_d$ – torque applied on the device coupling from stiffness [Nm]

$M_{fp} = F_f r_{fp}$ – torque applied on the pinion from tooth friction [Nm]

$M_{fg} = F_f r_{fg}$ – torque applied on the gear from tooth friction [Nm]

$F_n = k\left(r_{b1}\varphi_p + x_p - x_{py} - r_{b2}\varphi_g + x_g - x_{gy}\right) + c\left(r_{b1}\dot{\varphi}_p + \dot{x}_p - \dot{x}_{py} - r_{b2}\dot{\varphi}_g + \dot{x}_g - \dot{x}_{gy}\right)$ – normal force [N]

F_f – tooth friction force [N]

$F_d = \sqrt{F_n^2 + F_f^2}$ – resultant meshing force [N]

r_f – moment arm of sliding friction force [m]

$F_{kb1x} = k_{b1}x_{b1}$ – reaction force of bearing 1 from stiffness parallel to the x(LOA) axis [N] (Subscript 2, 3, 4 – bearing 2, bearing 3, bearing 4)

$F_{cb1x} = c_{b1}\dot{x}_{b1}$ – reaction force of bearing 1 from damping parallel to the x(LOA) axis [N]

2. Calculation of the dependency between the movement of gears along OLOA on the contact point on LOA

A change in the position of gear axis of rotation along the OLOA direction has impact on the distance between the meshing teeth. From the point of view of dynamic analysis, it is important to know a formula describing changes in the tooth distance along LOA depending on the movement of gears along OLOA. This affects dynamic forces. For clarity of the figure, below is given an example of the displacement of pinion axis of rotation when the center distance is increased without gear movement. Relationships will be derived for a general case describing the displacement of two gears or one gear only.

The nominal position of the gears is marked with a blue dashed line (Fig. 1). The teeth are in mesh at the pitch point C on LOA. According to Fig. 1, the pinion is displaced by a value y_p in the y axis direction. In effect, the distance between the gear axes is increased. To calculate a new center distance a_{w1}, it is convenient to divide the pinion displacement y_p into two separate displacements, e_p and f_p, according to a system of coordinates with the *e* and *f* axes:

$$a_{w1} = \left|O_{11}O_2\right| = \sqrt{\left(a_w + f_p - f_g\right)^2 + \left(e_p - e_g\right)^2} \tag{1}$$

where:

$a_w = \left|O_1O_2\right|$ – center distance of gears with shifted profiles,

O_2 – point of intersection with gear axis of rotation,

$f_p = y_p\cos\alpha_w$ – displacement of gear axis of rotation about the f axis,

$f_g = y_g\cos\alpha_w$ – displacement of gear axis of rotation about the f axis,

$e_p = y_p\sin\alpha_w$ – displacement of pinion axis of rotation about the e axis,

$e_g = y_g\sin\alpha_w$ – displacement of gear axis of rotation about the e axis.

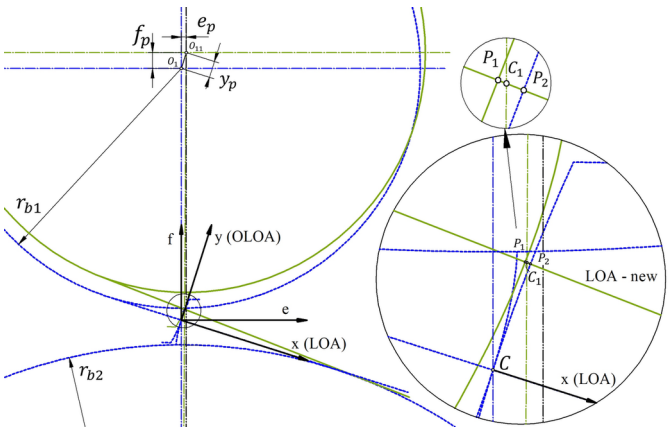

Fig. 1. Pinion displacement by a value y_p about the y axis, leading to a change in pinion axis of rotation position from O_1 to O_{11}

Changes in the center distance of gears have impact on tooth meshing conditions. The green line marks the new LOA. In the magnified image in Fig. 1 one can clearly see a clearance between the mating gear teeth (distance $\left|P_1P_2\right|$) at the contact point C before pinion displacement.

For convenience, the distance $\left|P_1P_2\right|$ can be divided into two sections. One is the pinion tooth distance P_1 from a new contact point C_1, while the other is the gear tooth distance P_2 from the contact point C_1. Fig. 2 shows the pinion along with the relationships enabling the determination of the $\left|P_1C_1\right|$ distance. It should be stressed

that the figure is not drawn to scale due to the fact that actual displacements are very small.

The angle ζ between the line connecting the gear center distance before displacement $|O_1O_2|$ and after displacement $|O_{11}O_2|$ is equal to:

$$\zeta = \sin^{-1}\left(\frac{e_p - e_g}{a_{w1}}\right) \tag{2}$$

Next, the angle $\measuredangle U_1O_{11}U_{11}$ denoted by β is calculated as:

$$\beta = \mathrm{inv}\alpha_{w1} - \mathrm{inv}\alpha_w - \zeta \tag{3}$$

where:

$\mathrm{inv}\alpha_{w1} = \tan\alpha_{w1} - \hat{\alpha}_{w1}$ is the involute function,

$\mathrm{inv}\alpha_w = \tan\alpha_w - \hat{\alpha}_w$ is the involute function,

$\hat{\alpha}_{w1} = \cos^{-1}\frac{r_{b1}}{r_{w11}}$ is the contact pressure angle after pinion displacement (for the center distance a_{w1}) [rad],

$\hat{\alpha}_w$ is the contact pressure angle before pinion displacement – nominal position (for the center distance a_w) [rad].

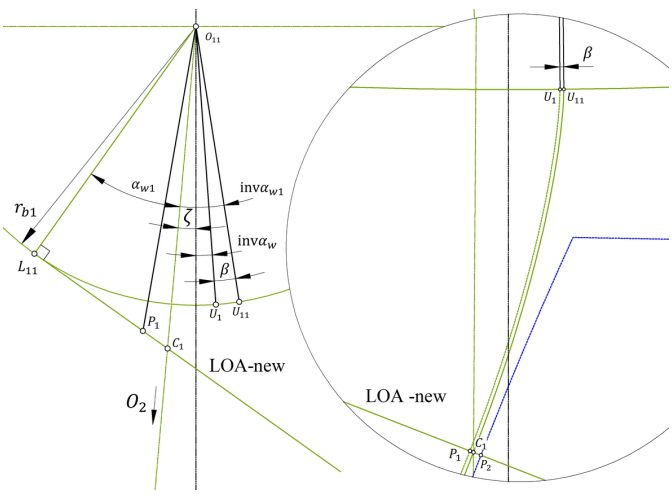

Fig. 2. Relationships for determining the pinion profile distance between P_1 and C_1

The distance $|P_1C_1|$ is equal to the arc length $\widehat{U_1U_{11}}$. This is due to the fact that the involute profile pitch is constant (involutes generated on the base circle are spaced by a constant distance measured tangentially to this circle).

$$|P_1C_1| = x_{py} = \hat{\beta} r_{b1} \tag{4}$$

where $\hat{\beta}$ is given in radians.

A similar approach can be adopted to calculate the distance $|P_2C_1|$. By knowing the distance $|P_1C_1|$, the distance between gear tooth profile and new contact point C_1 can be calculated as:

$$|P_2C_1| = x_{gy} = |P_1C_1|\frac{z_2}{z_1} \tag{5}$$

The total displacement resulting from the displacement of gears is:

$$|P_1P_2| = x_{pgy} = |P_1C_1| + |P_2C_1| \tag{6}$$

Formulas (4), (5) and (6) describe simultaneous displacement of two gears, one gear and a pinion. The displacement can be positive or negative about the y axis (OLOA). The gear teeth in contact can take any position on LOA. In all cases, whether the gear axis displacement along OLOA causes a decrease or increase in the center distance, this always results in a clearance between the mating teeth.

The above formulas were derived for a general case in which the gears have shifted profiles. If the gears are without this correction, the following parameters simplify to: $a_w = a$, $\alpha_w = \alpha$, $r_w = r$.

3. Simulation of the influence of gear parameters on the total displacement x_{pgy}

The displacement of gears along the OLOA direction can have different effects on the resultant distance between the mating teeth along LOA x_{pgy}. Tooth size and shape, contact ratio and center distance are the main parameters affecting x_{pgy} and thus will be investigated in this study. The following properties of gears were selected for simulations, depending on the case under analysis: m = 3 mm, $a_w = a = 100$ mm, z_p = 20, z_g = 20, $\alpha_w = 20°$. In all five cases (Fig. 3-7) only the pinion was displaced (y_p = – 200 µm ÷ 200 µm) along OLOA, which affected the nominal center distance.

Figure 3 illustrates the influence of module m. On changing this parameter, the center distance, gear diameters and tooth height change significantly too. The smaller the value of the module is, the greater the total displacement x_{pgy} becomes. This relationship is nonlinear. The maximum value x_{pgy} 2.7 µm is obtained for m = 1 mm and $y_p = -200$ µm or 200 µm.

The influence of the gear ratio u is presented in Figure 4. Different values of the gear ratio u are obtained by changing the number of gear teeth z_g = 16 ÷ 105, with the number of pinion teeth maintained constant at z_p = 20. By changing the number of gear teeth, the gear diameter, center distance and contact ratio change, too. The smaller value of the gear ratio is, the greater the total displacement x_{pgy} becomes. This relationship is nonlinear. The maximum value x_{pgy} 1.1 µm is obtained for u = 0.8 and y_p = – 200 µm or 200 µm.

The pressure angle α is another investigated parameter. In this case, other parameters do not change like in previous cases, the only exception being the base circle dimension. The smaller the pressure angle value is, the greater the total displacement x_{pgy} becomes. This relationship is nonlinear (Fig. 5). The maximum value x_{pgy} 1.8 µm is obtained for α = 11° and y_p = – 200 µm or 200 µm.

The last examined parameter is the number of the gear teeth z_p, z_g. Their number is the same ($z_p = z_g$ = 18 ÷ 60) and has impact on the dimension of gears and center distance. To obtain more general results,

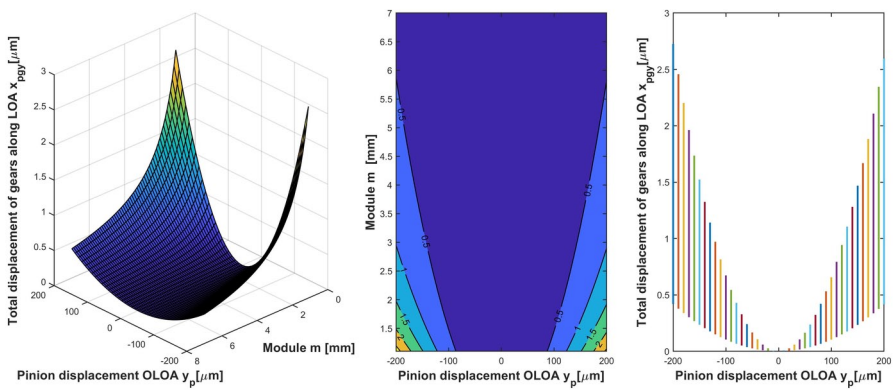

Fig. 3. Relationship between module m, pinion displacement y_p and total tooth displacement x_{pgy}, presented in three types of diagrams

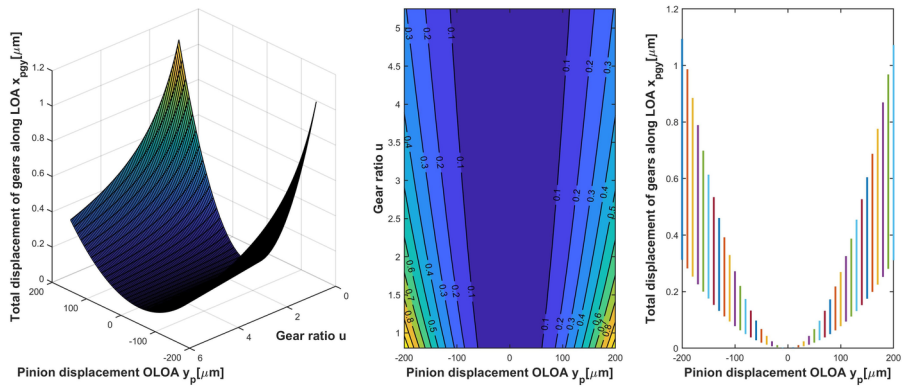

Fig. 4. Relationship between gear ratio u, pinion displacement y_p and total tooth displacement x_{pgy}, , presented in three types of diagrams

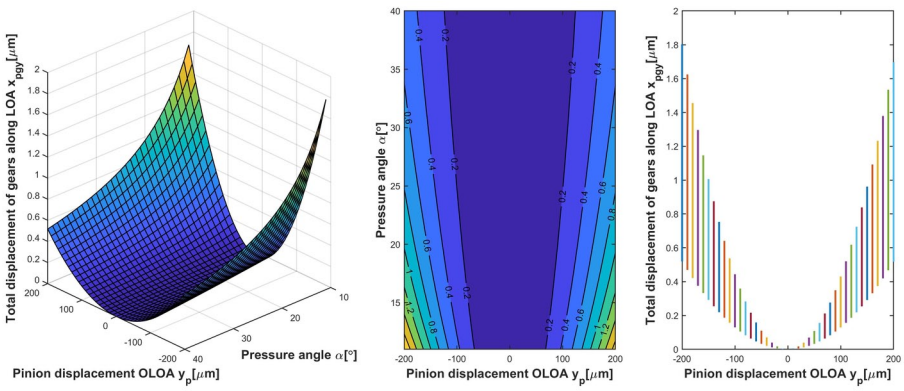

Fig. 5. Relationship between pressure angle α, pinion displacement y_p and total tooth displacement x_{pgy} , presented in three types of diagrams

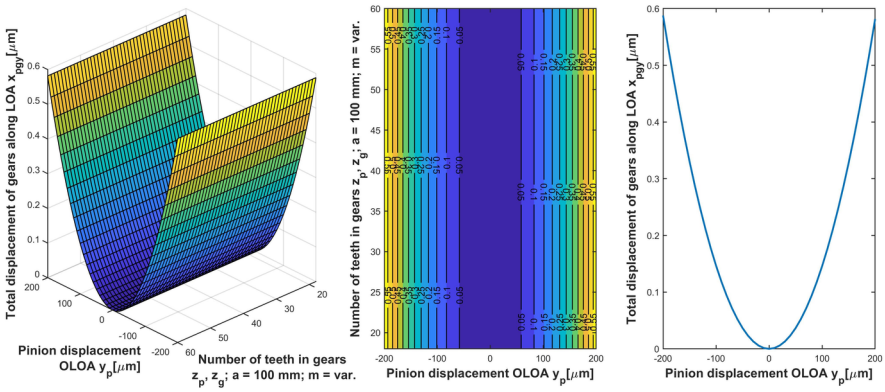

Fig. 6. Relationship between the number of gear teeth z_p, z_g (a = 100 mm, m = var.), pinion displacement y_p and total tooth displacement x_{pgy} , presented in three types of diagrams

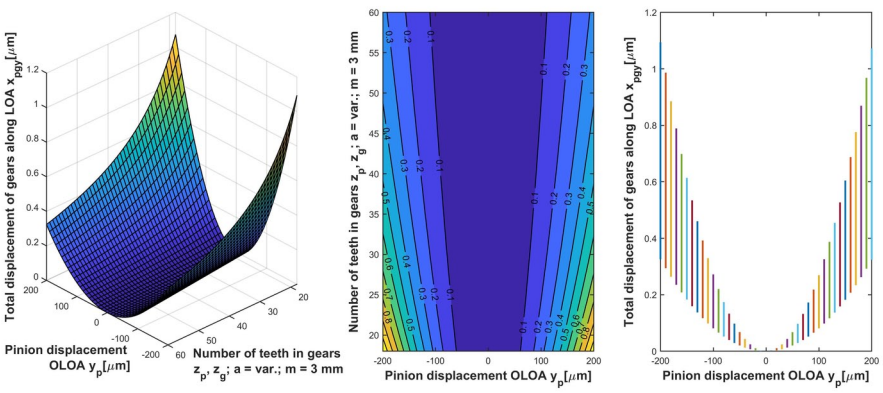

Fig. 7. Relationship between the number of gear teeth z_p, z_g (a = var., m = 3 mm), pinion displacement y_p and total tooth displacement x_{pgy} , presented in three types of diagram

two variants are considered. In the first one (Fig. 6), the center distance *a* has a constant value of 100 mm, hence the module *m* must be changed. The total tooth displacement x_{pgy} does not depend on the number of teeth in this case.

In the second variant, the module *m* is maintained constant at 3 mm, therefore the center distance must vary. Under these conditions, the total tooth displacement x_{pgy} depends on the number of gear teeth. The smaller the number of teeth is, the greater the total displacement x_{pgy} becomes. This relationship is nonlinear (Fig. 7). The maximum value x_{pgy} 1.1 μm is obtained for $z_p = z_g = 18$ and $y_p = -200$ μm or 200 μm.

It can be seen that the total tooth displacement x_{pgy} is not the same despite the identical pinion displacement y_p along the positive and negative sense of the *y* axis, which is especially visible in Figure 5. If the pinion displacement along OLOA causes a decrease in the center distance (negative value), its impact on the total tooth displacement is greater. The same relationship can be observed for the gears. It makes no difference whether one gear or two gears move along the OLOA direction. The resulting center distance is a factor affecting the total tooth displacement x_{pgy}. This conclusion can be drawn from Equation (1).

4. Simulation of spur gears for different values of tooth friction coefficient and bearing stiffness

To analyze the influence OLOA displacement of gears on their dynamics, a simulation was performed. One of the situations in which gear displacement along OLOA can be significant is when the force in a radial direction is high. This situation occurs during scuffing. The tooth friction force can achieve significant values as a result of this phenomenon. Nine cases of friction coefficient μ were considered with a step changed every 0.1, from 0.02 to 0.82. Bearing stiffness has a great impact on gear displacement, too. Four values of the bearing stiffness k_b were analyzed: $1.1 \cdot 10^8$ N/m; $1.1 \cdot 10^{8,5}$ N/m; $1.1 \cdot 10^9$ N/m; $1.1 \cdot 10^{9,5}$ N/m. The stiffness values were the same for all bearings and in all directions. Parameters of gear unit and other components are presented in Table 1 and 2.

The simulation was performed on a 12 DOF model (Fig. 8). The model consisted of rigid elements. Every shaft had 5 DOF. The gears were located in the middle of the bearings. The gear unit was connected by couplings with a motor and output device. Dynamic equations were as follows:

$$I_m\ddot{\varphi}_m + M_{cm} + M_{km} = T_m \tag{7}$$

$$I_p\ddot{\varphi}_p + M_{cp} + M_{kp} = M_{cm} + M_{km} + M_{fp} \tag{8}$$

$$I_g\ddot{\varphi}_g + M_{cd} + M_{kd} + M_{fg} = M_{cg} + M_{kg} \tag{9}$$

$$I_d\ddot{\varphi}_d + T_d = M_{cd} + M_{kd} \tag{10}$$

$$F_{kb1x}l_p + F_{cb1x}l_p + m_p\ddot{x}_{pCoM}\left(l_p - l_{p2}\right) - I_{px}\ddot{\theta}_{px} = F_n\left(l_p - l_{p1}\right) \tag{11}$$

$$F_{kb2x}l_p + F_{cb2x}l_p + m_p\ddot{x}_{pCoM}l_{p2} + I_{px}\ddot{\theta}_{px} = F_n l_{p1} \tag{12}$$

$$F_{kb3x}l_g + F_{cb3x}l_g + m_g\ddot{x}_{gCoM}\left(l_g - l_{g2}\right) + I_{gx}\ddot{\theta}_{gx} = F_n\left(l_g - l_{g1}\right) \tag{13}$$

$$F_{kb4x}l_g + F_{cb4x}l_g + m_g\ddot{x}_{gCoM}l_{g2} - I_{gx}\ddot{\theta}_{gx} = F_n l_{g1} \tag{14}$$

$$F_{kb1y}l_p + F_{cb1y}l_p + m_p\ddot{y}_{pCoM}\left(l_p - l_{p2}\right) - I_{py}\ddot{\theta}_{py} = F_f\left(l_p - l_{p1}\right) \tag{15}$$

$$F_{kb2y}l_p + F_{cb2y}l_p + m_p\ddot{y}_{pCoM}l_{p2} + I_{py}\ddot{\theta}_{py} = F_f l_{p1} \tag{16}$$

$$F_{kb3y}l_g + F_{cb3y}l_g + m_g\ddot{y}_{gCoM}\left(l_g - l_{g2}\right) + I_{gy}\ddot{\theta}_{gy} = F_f\left(l_g - l_{g1}\right) \tag{17}$$

$$F_{kb4y}l_g + F_{cb4y}l_g + m_g\ddot{y}_{gCoM}l_{g2} - I_{gy}\ddot{\theta}_{gy} = F_f l_{g1} \tag{18}$$

Detailed information about tooth stiffness, Coulomb friction and other details concerning the analytical model can be found in [10, 11].

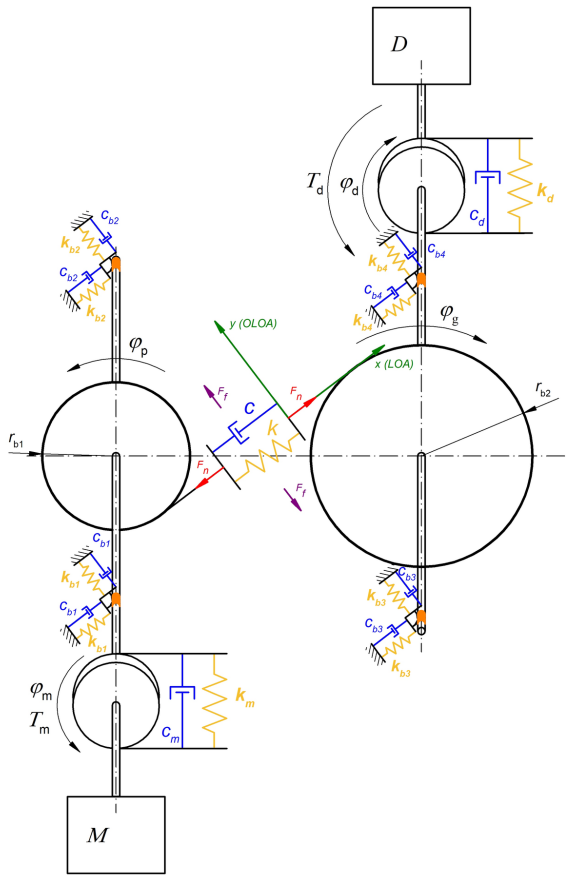

Fig. 8. Analytical model of gear unit with motor M and output device D

Table 1. Properties of gears

Parameter	Pinion	Gear
Number of teeth	$z_p = 20$	$z_g = 20$
Module [mm]	$m = 2$	
Pressure angle [°]	$\alpha_0 = 20$	
Contact ratio	$\varepsilon = 1{,}557$	
Moment of inertia (pinion/gear, shaft and half of motor/device coupling) [kgm^2]	$I_p = 0.0033315$; $I_{px} = I_{py} = 0.0117285$	$I_g = 0033315$; $I_{gx} = I_{gy} = 0.0117285$
Mesh damping [Ns/m]	$c = 40$	
Initial angular speed [rad/s]	$\omega_p = 157{,}0796$ ($n_p = 1500$ rpm)	$\omega_g = 157.0796$
Max stiffness of one pair of teeth [N/m]	$380 \cdot 10^6$	

Table 2. Properties of other components

Parameter	Motor rotor	Device rotor
Moment of inertia [kgm^2]	$I_m = 0.075$	$I_d = 0.12$
Torque [Nm]	$T_m = 31.83$	$T_d = 31.83$
Initial angular speed [rad/s]	$\omega_m = 157.0796$ ($n_m = 1500$ rpm)	$\omega_d = 157.0796$
	Motor coupling	Device coupling
Stiffness [N/m]	$k_m = 9.3 \cdot 10^4$	$k_d = 9.3 \cdot 10^4$
Damping [Ns/m]	$c_m = 10$	$c_d = 10$
	Bearings	
Damping [Ns/m]	$c_b = 40$	

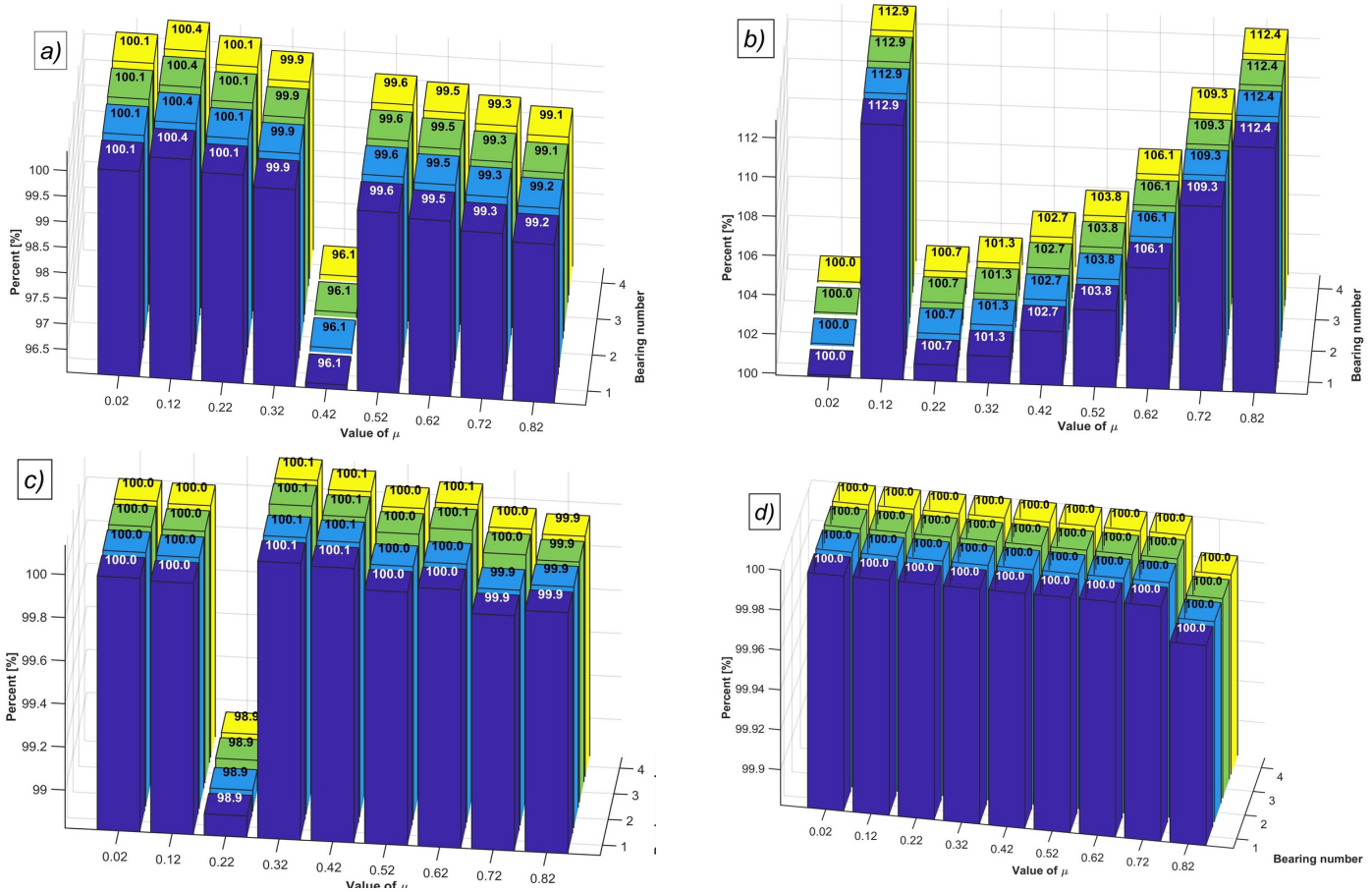

Fig. 9. Percentage change in the resultant reaction force of bearings obtained by considering gear displacement along OLOA and its influence on gear meshing. Results were obtained for the following bearing stiffness values: a) $1{,}1 \cdot 10^{8}$ N/m, b) $1{,}1 \cdot 10^{8{,}5}$ N/m, c) $1{,}1 \cdot 10^{9}$ N/m, d) $1{,}1 \cdot 10^{9{,}5}$ N/m

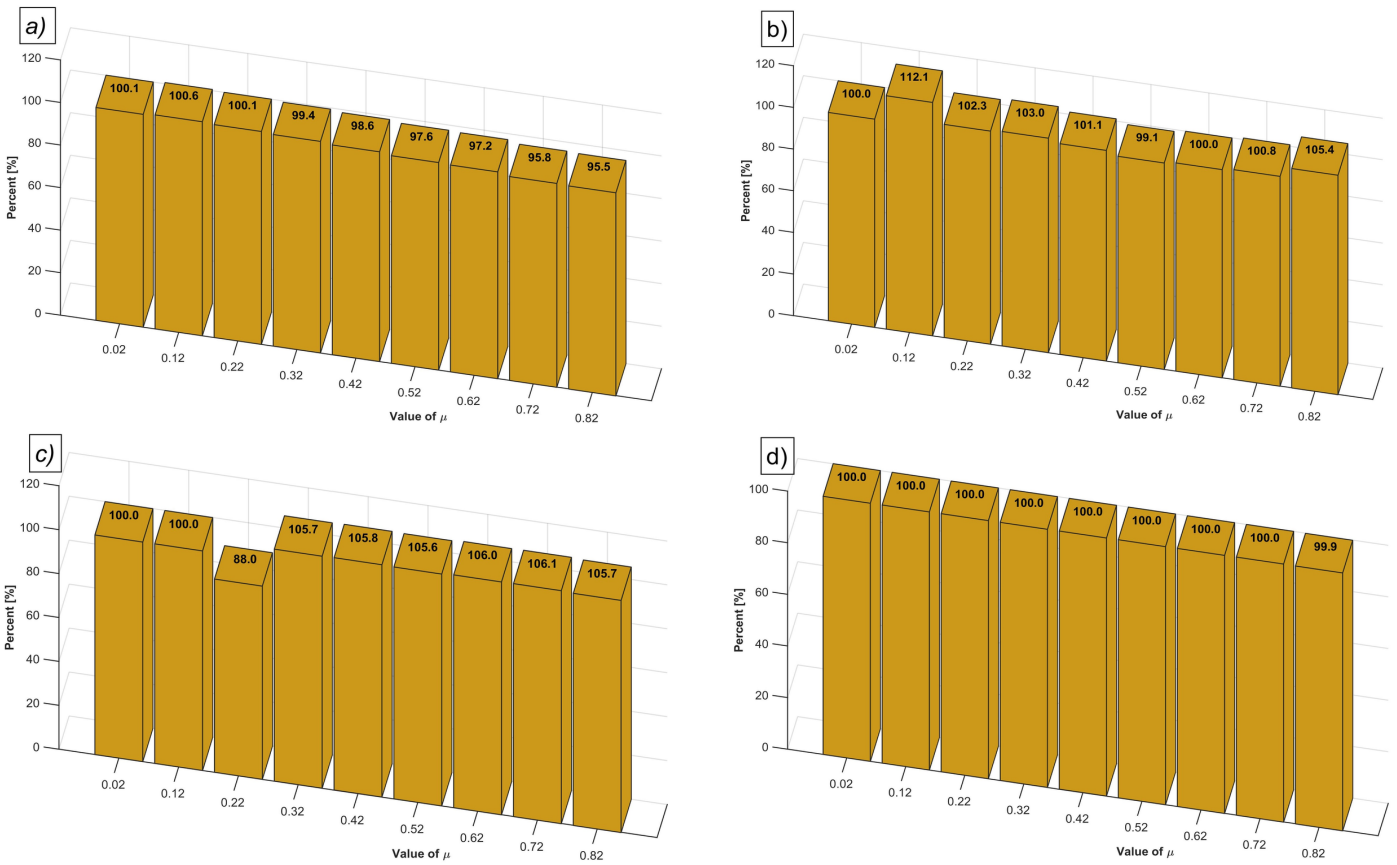

Fig. 10. Percentage change in the resultant meshing force obtained by considering gear displacement along OLOA and its influence on gear meshing. Results were obtained for the following bearing stiffness values: a) $1{,}1 \cdot 10^{8}$ N/m, b) $1{,}1 \cdot 10^{8{,}5}$ N/m, c) $1{,}1 \cdot 10^{9}$ N/m, d) $1{,}1 \cdot 10^{9{,}5}$ N/m

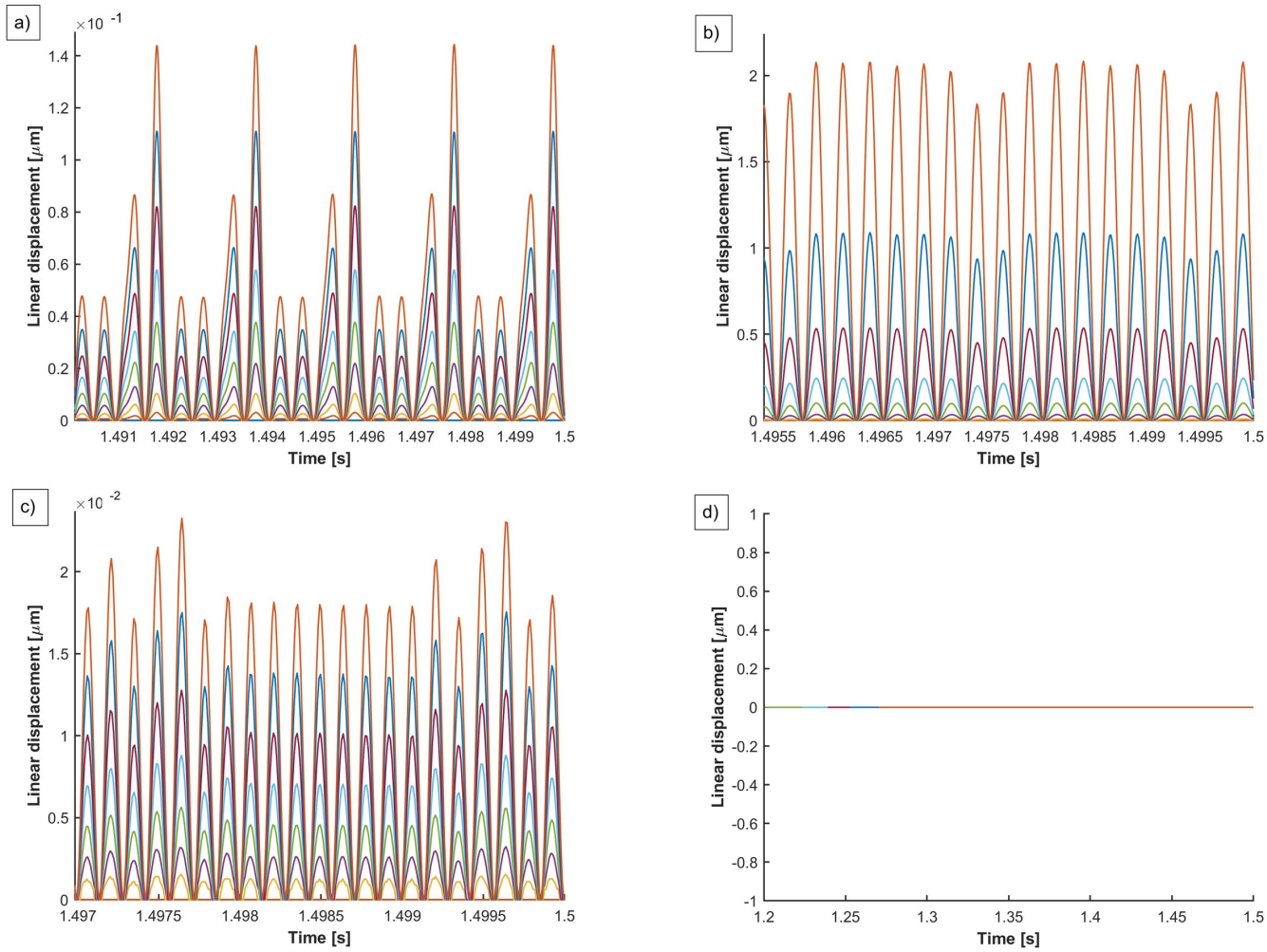

Fig. 11. Total displacement x_{pgy} (increased distance) of the pinion and gear teeth in mesh along the LOA direction as caused by gear displacement along OLOA. Results were obtained for the following bearing stiffness values: a) $1.1 \cdot 10^{8}$ N/m, b) $1.1 \cdot 10^{8,5}$ N/m, c) $1.1 \cdot 10^{9}$ N/m, d) $1.1 \cdot 10^{9,5}$ N/m

The reaction force in Fig. 9a is slightly higher than the nominal value for the coefficient of friction ranging from 0.2 to 0.22. For a higher coefficient of friction, the reaction force decreases below the nominal value (nominal value means, that result is obtained without taking into account influence of OLOA displacement of gears on LOA direction). The situation changes when the bearing stiffness is increased (Fig. 9b). For this case, the reaction force is always higher than the nominal value. The difference in the reaction force values in Fig. 9c is very small and in Fig. 9d it is negligible.

The resultant meshing force is a load on the bearings, thus the results in Fig. 9 and Fig. 10 show very similar trends. The maximum difference between the resultant meshing force and the nominal value is 12.1% for the bearing stiffness of $1.1 \cdot 10^{8,5}$ N/m (Fig. 10b). For the bearing stiffness equal to $1.1 \cdot 10^{8}$ N/m the difference in the resultant meshing is 5.1% (Fig. 10a), while for the bearing stiffness of $1.1 \cdot 10^{9}$ the difference is 18.1% (Fig. 10c). In Fig. 10d one can only observe one slight change for the highest friction coefficient value.

Examples of waveforms of the total displacement x_{pgy} are presented in Fig. 11. Different colors mark different values of the friction coefficient. The value x_{pgy} is always positive. The maximum displacement is obtained for the bearing stiffness value equal to $1.1 \cdot 10^{8,5}$ N/m. A straight line in Fig. 11d means that displacement does not occur.

5. Conclusions

This study investigated the effect of varying the center distance along OLOA on the gear tooth position along LOA. An exact formula has been derived for a general case of spur gears with shifted profiles. It has been found that changes in the nominal center distance result in an increased distance between the working surfaces of the gear teeth, i.e. normal backlash. The presented method for determining the distance between the working tooth surface along LOA (normal backlash) is suitable not only for the OLOA direction, but for any other directions, too.

A simulation was performed to establish the relationship between gear parameters and total tooth displacement. It has been found that the module has the greatest impact out of all tested parameters. The second highest result was obtained for the pressure angle. Given that most gear parameters are interdependent, it is not easy to formulate general conclusions. Nonetheless, the movement of gears along the OLOA direction has a greater impact on the movement of the mating teeth along LOA for small gears with a lower gear ratio and a smaller number of teeth.

The effect of the total displacement x_{pgy} on the dynamic behavior of gears was investigated. Based on an analytical model of reaction forces for bearings, resultant meshing force and waveforms of total displacement x_{pgy} were presented. The reaction forces of bearings and the resultant meshing force are strictly interdependent, and the trends obtained for these two parameters are very similar. In the presented example, the reaction forces were higher by more 12 %, and the resultant meshing force was higher, too. The trends are not linear, so a higher frictional force does not always mean that the bearing reaction forces and resultant meshing force will be higher too. It has been found that bearing stiffness has a great impact on the total displacement x_{pgy} and dynamic behavior of gears.

References

1. Cao H, Shi F, Li Y et al. Vibration and stability analysis of rotor-bearing-pedestal system due to clearance fit. Mechanical Systems and Signal Processing 2019; 133: 106275, https://doi.org/10.1016/j.ymssp.2019.106275.
2. Chen G, Qu M. Modeling and analysis of fit clearance between rolling bearing outer ring and housing. Journal of Sound and Vibration 2019; 438: 419-440, https://doi.org/10.1016/j.jsv.2017.11.004.
3. Chernets M. Method of calculation of tribotechnical characteristics of the metal-polymer gear, reinforced with glass fiber, taking into account the correction of tooth. Eksploatacja i Niezawodnosc - Maintenance and Reliability 2019; 21(4): 546-552, https://doi.org/10.17531/ein.2019.4.2.
4. Cirelli M, Giannini O, Valentini P P, Pennestrì E. Influence of tip relief in spur gears dynamic using multibody models with movable teeth. Mechanism and Machine Theory 2020, https://doi.org/10.1016/j.mechmachtheory.2020.103948.
5. Dai H, Long X, Chen F, Xun C. An improved analytical model for gear mesh stiffness calculation. Mechanism and Machine Theory 2021; 159: 104262, https://doi.org/10.1016/j.mechmachtheory.2021.104262.
6. Fernandez-del-Rincon A, Garcia P, Diez-Ibarbia A et al. Enhanced model of gear transmission dynamics for condition monitoring applications: Effects of torque, friction and bearing clearance. Mechanical Systems and Signal Processing 2017; 85: 445-467, https://doi.org/10.1016/j.ymssp.2016.08.031.
7. Guangjian W, Lin C, Li Y, Shuaidong Z. Research on the dynamic transmission error of a spur gear pair with eccentricities by finite element method. Mechanism and Machine Theory 2017; 109: 1-13, https://doi.org/10.1016/j.mechmachtheory.2016.11.006.
8. Isaacson A C, Wagner M E. Oil-off characterization method using in-situ friction measurement for gears operating under loss-of-lubrication conditions. American Gear Manufacturers Association Fall Technical Meeting 2018: 46-54.
9. ISO 1328-2 1997 - Cylindrical gears-ISO system of accuracy.
10. Jedlinski L. Analysis of the influence of gear tooth friction on dynamic force in a spur gear. Journal of Physics: Conference Series 2021, https://doi.org/10.1088/1742-6596/1736/1/012011.
11. Jedliński Ł. New Analytical Model of Spur Gears with 5 DOF Shafts and its Comparison with Other DOF Models. Advances in Science and Technology Research Journal 2021; 15(1): 79-91, https://doi.org/10.12913/22998624/130661.
12. Liu C, Yin X, Liao Y et al. Hybrid dynamic modeling and analysis of the electric vehicle planetary gear system. Mechanism and Machine Theory 2020; 150: 103860, https://doi.org/10.1016/j.mechmachtheory.2020.103860.
13. Liu H, Zhang C, Xiang C L, Wang C. Tooth profile modification based on lateral- torsional-rocking coupled nonlinear dynamic model of gear system. Mechanism and Machine Theory 2016; 105: 606-619, https://doi.org/10.1016/j.mechmachtheory.2016.07.013.
14. Liu Z, Liu Z, Zhao J, Zhang G. Study on interactions between tooth backlash and journal bearing clearance nonlinearity in spur gear pair system. Mechanism and Machine Theory 2017; 107: 229-245, https://doi.org/10.1016/j.mechmachtheory.2016.09.024.
15. Michalczewski R, Kalbarczyk M, Michalak M et al. New Scuffing Test Methods for the Determination of the Scuffing Resistance of Coated Gears. Tribology - Fundamentals and Advancements 2013, https://doi.org/10.5772/54569.
16. Mohsenzadeh R, Shelesh-Nezhad K, Chakherlou T N. Experimental and finite element analysis on the performance of polyacetal/carbon black nanocomposite gears. Tribology International 2021; 160: 107055, https://doi.org/10.1016/j.triboint.2021.107055.
17. Shi J fei, Gou X feng, Zhu L yun. Modeling and analysis of a spur gear pair considering multi-state mesh with time-varying parameters and backlash. Mechanism and Machine Theory 2019; 134: 582-603, https://doi.org/10.1016/j.mechmachtheory.2019.01.018.
18. Skrickij V. Viktor Skrickij Marijonas Bogdevičius Rasa Žygienė. Evaluation of the spur gear condition using extended frequency range. Eksploatacja i Niezawodnosc - Maintenance and Reliability 2017; 19(3): 476-484, https://doi.org/10.17531/ein.2017.3.19.
19. Tiwari M, Gupta K, Prakash O. Effect of radial internal clearance of a ball bearing on the dynamics of a balanced horizontal rotor. Journal of Sound and Vibration 2000; 238(5): 723-756, https://doi.org/10.1006/jsvi.1999.3109.
20. Tomović R. Calculation of the necessary level of external radial load for inner ring support on q rolling elements in a radial bearing with internal radial clearance. International Journal of Mechanical Sciences 2012; 60(1): 23-33, https://doi.org/10.1016/j.ijmecsci.2012.04.002.
21. Walha L, Fakhfakh T, Haddar M. Nonlinear dynamics of a two-stage gear system with mesh stiffness fluctuation, bearing flexibility and backlash. Mechanism and Machine Theory 2009; 44(5): 1058-1069, https://doi.org/10.1016/j.mechmachtheory.2008.05.008.
22. Wang S, Zhu R. Theoretical investigation of the improved nonlinear dynamic model for star gearing system in GTF gearbox based on dynamic meshing parameters. Mechanism and Machine Theory 2021; 156: 104108, https://doi.org/10.1016/j.mechmachtheory.2020.104108.
23. Wang Z, Zhu C. A new model for analyzing the vibration behaviors of rotor-bearing system. Communications in Nonlinear Science and Numerical Simulation 2020; 83: 105130, https://doi.org/10.1016/j.cnsns.2019.105130.
24. Xiao Y, Fu L, Luo J et al. Nonlinear dynamic characteristic analysis of a coated gear transmission system. Coatings 2020; 10(1): 4-6, https://doi.org/10.3390/coatings10010039.
25. Yi Y, Huang K, Xiong Y, Sang M. Nonlinear dynamic modelling and analysis for a spur gear system with time-varying pressure angle and gear backlash. Mechanical Systems and Signal Processing 2019; 132: 18-34, https://doi.org/10.1016/j.ymssp.2019.06.013.
26. Zhang X, Zhao J. Compound fault detection in gearbox based on time synchronous resample and adaptive variational mode decomposition. Eksploatacja i Niezawodnosc - Maintenance and Reliability 2020; 22(1): 161-169, https://doi.org/10.17531/ein.2020.1.19.
27. Zhao Z, Han H, Wang P et al. An improved model for meshing characteristics analysis of spur gears considering fractal surface contact and friction. Mechanism and Machine Theory 2021; 158: 104219, https://doi.org/10.1016/j.mechmachtheory.2020.104219.